JOURNAL OF CATALYSIS 148, 181–193 (1994)

Investigation of the Role of Nickel and the Effect of Gas Phase Sulfur Compounds on the Performance of Ni–Mo/γ-Al_2O_3 Hydrodenitrogenation Catalysts

Umit S. Ozkan,[1] Liping Zhang, Shuangyao Ni, and Edgar Moctezuma[2]

The Ohio State University, Department of Chemical Engineering, Columbus, Ohio 43210

Received November 18, 1993; revised February 25, 1994

A series of γ-Al_2O_3-supported molybdenum and nickel sulfide catalysts was prepared in order to investigate the role of the nickel promoter and the effect of the sulfur feed compounds on the hydrodenitrogenation (HDN) performance of Ni–Mo/γ-Al_2O_3 catalysts. The reactions performed were pyridine HDN, thiophene HDS, HDN in the presence of thiophene, and HDN in the presence of H_2S. The catalysts were characterized using laser Raman spectroscopy, X-ray diffraction, X-ray photoelectron spectroscopy, BET surface area measurement, and temperature-programmed desorption of H_2S, thiophene, and pyridine. The results of the reaction studies and characterization experiments are combined with earlier reports in the literature to propose an explanation of the role of nickel and gas phase sulfur compounds in pyridine HDN network.

INTRODUCTION

Sulfided Mo catalysts supported on γ-Al_2O_3 with Co or Ni as the promoter have long been used in the industrial hydrotreating processes. Extensive studies have been conducted on the subject and have been summarized in several reviews (1–4), with the main emphasis having been on Co–Mo catalysts in hydrodesulfurization (HDS) reactions. Recently, there has been an increased need to process heavy fuels and low-quality stocks which contain larger quantites of nitrogen compounds than traditional petroleum stocks. Thus, a better understanding of the hydrodenitrogenation (HDN) catalysis is required, especially over Ni–Mo catalyst systems since it has been found to be more active than Co–Mo catalysts in HDN reactions.

Although HDN over Ni–Mo/γ-Al_2O_3 systems has been extensively studied (1, 5–14), questions still remain about the nature of the promotion effect by nickel and the role of sulfur compounds in the feed stream. The presence of a synergistic role of Ni on catalytic activity of Mo appears to be conditional. While some researchers reported a strong synergy between Mo and the Ni promoter (9, 12), others found no synergy at all for the system (15). Perot and co-workers (16, 17) and Ledoux and Djellouli (12) found that sulfided Ni–Mo catalysts showed a synergistic effect at high hydrogen pressure and in the presence of hydrogen sulfide.

Sulfur-containing compounds in the reaction feed have been shown to affect the HDN activity considerably for Ni–Mo/γ-Al_2O_3 catalysts (8–12, 16–18). In contrast to the inhibitive effect of nitrogen compounds on thiophene HDS, sulfur compounds exhibit a dual effect on pyridine HDN (9). At low temperatures, sulfur compounds show a moderate inhibition effect on pyridine HDN, while at high temperatures they enhance HDN activity considerably. The temperature at which this transformation occurs depends on the system pressure, with the transformation taking place at lower temperatures as the system pressure is increased. Thus far, a complete understanding of the catalytic phenomena responsible for the observed results has not been reached. Laine (19) proposed that HDN activity is enhanced by H_2S because ring opening is promoted through a nucleophilic attack by gas phase H_2S on adsorbed nitrogen cycles. Nelson and Levy (20) suggested that C–N bond cleavage involves Hofmann degradation promoted by H^+ from dissociated H_2S on the catalyst surface. Satterfield *et al.* (9) summarized that sulfur-containing compounds promote HDN in several ways: by keeping the catalysts fully sulfided at the reaction surface, by increasing the surface acidity of the catalyst, and by decreasing the adsorptivity of basic nitrogen compounds (aliphatic amines) on the catalyst. Olalde and Perot (16) explained the role of sulfur as follows: H_2S or its precursor in the feed contributes by increasing or maintaining the degree of surface sulfidation of the catalyst; consequently the nature of the catalytic surface active sites is modified by the change in the surface composition. They also sug-

[1] To whom correspondence should be addressed. E-mail: OZKAN.1@OSU.EDU.

[2] Present address: Universidad Autonoma de San Luis Potosi, Facultad de Ciencias Quimicas, San Luis Potosi, S.L.P., Mexico.

0021-9517/94 $6.00

gested that sulfur participates in the reaction pathway by creating new reactive intermediates.

The general phase structure of Ni–Mo/γ-Al_2O_3 catalysts is expected to be similar to the widely accepted Ni–Mo–S structure proposed by Topsøe and co-workers for HDS reactions (3, 21, 22). In the Ni–Mo–S structure, Mo exists in slabs of a MoS_2-like phase with Ni atoms decorating Mo atoms at the edges of the platelets. Although this phase structure is well accepted, the exact form and characteristics of the active sites have not yet been fully determined. Until now, the suggested active sites for HDN have not fully accounted for the effects of Ni. Ledoux *et al.* (23) suggested that, for HDS only, the Mo at the edge sites is active, and the major role of nickel is to stabilize the MoS_2 phase structure and maintain its dispersion on the support. Topsøe and Clausen (3) suggested that the role of nickel in HDS is to form vacancy sites which have a much higher intrinsic HDS activity than unpromoted Mo sites, but they also mentioned that unpromoted Mo sites might play an important role for other reactions.

X-ray photoelectron spectroscopy (XPS) is used to a limited extent to determine the surface composition and the coordination state of the constituent metal atoms on HDS and HDN catalysts. The few XPS studies conducted for Ni–Mo catalysts thus far are not conclusive. Some researchers (24–26) observed higher binding energies for Co and Ni in contact with Mo than for bulk Co or Ni, but Radchenko *et al.* (27) reported lower binding energies for the same system.

In this work, sulfided forms of γ-Al_2O_3-supported Ni, Mo, and bimetallic Ni–Mo catalysts were used to perform individual and simultaneous thiophene HDS and pyridine HDN studies. Characterization of the catalysts was performed before and after sulfiding, before and after reaction, and in some cases *in situ*. The characterization methods used were laser Raman spectroscopy, X-ray diffraction, X-ray photoelectron spectroscopy, BET surface area, and temperature-programmed desorption. The characterization results were combined with reaction data to gain insight about the HDN reaction pathway and the nature of surface active sites.

EXPERIMENTAL

Catalyst Preparation

The series of alumina-supported NiO, MoO_3, and NiO–MoO_3 catalysts used in these studies were prepared by wet co-impregnation of alumina (γ-Al_2O_3) (Harshaw–Filtre) with aqueous solutions of nickel nitrate ($Ni(NO_3)_2 \cdot 6H_2O$) (Mallinckrodt) and ammonium heptamolybdate ($(NH_4)_6Mo_7O_{24} \cdot 4H_2O$) (Fisher). A pH of 8 was maintained during impregnation. After impregnation, the catalyst precursor was dried under vacuum, then calcined under a steady flow of pure oxygen at 500°C for 4 h. Prior to all reactions, the catalysts were sulfided *in situ* at 400°C under a flow of 10% H_2S/H_2 for 10 h. Catalyst compositions are reported as weight percentage of the oxide precursor following the convention commonly used in the literature.

BET, LRS, and XRD

The surface areas of the catalysts were measured using BET method with a Micromeritics AccuSorb 2100E instrument. Laser Raman spectra of the catalyst samples were obtained with a laser Raman spectrometer (SPEX model 1403 Ramalog 9-I spectrometer) which used a 5-W Argon ion laser (Spectra Physics, model 2016) as the excitation source. X-ray powder diffraction patterns were obtained using a Scintag PAD-V diffractometer with Cu$K\alpha$ radiation (λ = 1.5432 Å) as the X-ray source.

Reaction Studies

Thiophene HDS, pyridine HDN, and simultaneous HDS/HDN reactions were carried out in a 4-mm I.D. stainless steel flow reactor. The reactor was always loaded such that the total surface area of the catalyst was 50 m^2. Reaction temperatures were in the range of 320–400°C and pressure was 100 psig for all runs. The feed H_2 flow rate was controlled by a Tylan mass flow controller (model FC-280) at 70 cm^3(STP)/min. Thiophene and pyridine were introduced using a bubbler system and mole percentages in the reaction feed were kept at 0.87 mol% each in H_2, as verified by GC analysis. H_2S was introduced and maintained by a mass flow controller from a premixed supply of 10% H_2S in H_2. The feed and product streams were analyzed by an on-line HP 5890A gas chromatograph with both TCD and FID detectors. The reactant conversion rates and the product yields are expressed in units of μmol/min-m^2. Reaction data were collected after 3 h on-line when steady state had been achieved. The conversion and yield data were reproducible within 5%. Further details of reaction studies have been reported elsewhere (18).

XPS Measurements

X-ray photoelectron spectroscopy measurements of the catalysts were performed using a Physical Electronics/Perkin–Elmer (model 550) ESCA/Auger spectrometer operated at 15 kV and 20 mA with Mg$K\alpha$ radiation (1253.6 eV). Binding energies were referenced to Al 2*p* of 74.4 eV and determined with a precision of 0.1 eV. The XPS peak area ratios were determined by integrating areas of Mo 3*d*, Ni 2*p*, Al 2*p*, and S 2*p*, using PhiMat 3.1 software on an IMB PC.

XPS characterization of the catalysts was conducted

before and after sulfidation, and after the catalysts had been on-line for 5 h through HDS, HDN, or simultaneous HDS/HDN reactions at 400°C. Sulfided and postreaction catalyst samples were cooled to room temperature under a He flow, sealed with valves located on both ends of the reactor tube, and transferred into the XPS chambers without exposure to atmosphere. For XPS sample preparation, samples were mounted on double-sided sticky tape in an argon-atmosphere glove box.

Temperature Programmed Desorption

TPD of H_2S after sulfidation over the γ-Al_2O_3 support, 10%NiO, 20%MoO_3, and 3%NiO–15%MoO_3 catalysts was carried out in a temperature-programmed characterization system which was designed and built in our laboratories and which was described previously (28). The samples were sulfided *in situ* following the same procedure as the one used prior to the reaction studies, then cooled to 25°C under a flow of the same sulfiding gas mixture. After being flushed with helium for 30 min, the samples were heated to 850°C at a rate of 5°C/min under a 50 cm^3(STP)/min helium flow. The composition of the effluent gas was analyzed continuously by a mass spectrometer (Hewlett–Packard, MS Engine 5989A).

Post-reaction TPD of thiophene and pyridine was carried out *in situ* over the three catalyst samples after individual or simultaneous HDS and HDN reactions at 400°C for 5 h. The samples were cooled under He to 40°C, then heated to 650°C at a rate of 5°C/min with 50 cm^3(STP)/min helium as the carrier gas. The composition of the effluent gas was analyzed by on-line GC every 4 min to generate the TPD curve and to obtain the amount of desorbed sulfur- or nitrogen-containing gas.

RESULTS

Characterization of Oxidic Catalysts

The BET surface area of the catalysts used in these studies was 183, 165, 184, and 195 m^2/g, respectively, for the weight loadings of 10% NiO, 20% MoO_3, 3% NiO–15% MoO_3, and pure alumina, and was in the range of 162 to 195 m^2/g for other samples.

Laser Raman spectra of the oxidic samples (Fig. 1) showed the presence of crystalline MoO_3 at 15 and 20 wt% loading levels for the monometallic Mo samples through the appearance of bands at 820 cm^{-1} and 996 cm^{-1}. However, evidence for the presence of surface polymolybdates was also apparent in these samples through a band around 952 cm^{-1}, in agreement with previous reports (29–31). For NiO–MoO_3, the bands at 820 and 996 cm^{-1} disappeared and the band at 952 cm^{-1} was shifted to 960 cm^{-1} indicating a better dispersion of the catalyst and a possible interaction between Ni and Mo species in forming the polymolybdates species.

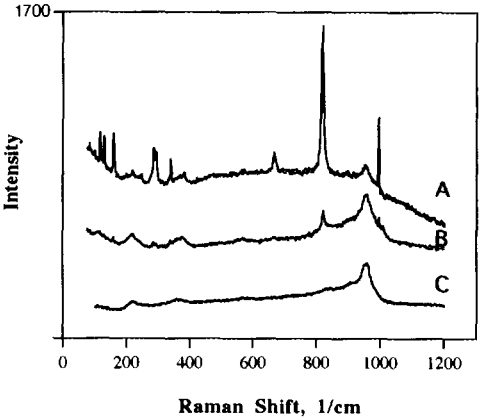

FIG. 1. Laser raman spectra of (A) 20% MoO_3/γ-Al_2O_3, (B) 15% MoO_3/γ-Al_2O_3, and (C) 3% NiO–15% MoO_3/γ-Al_2O_3.

The X-ray diffraction patterns of γ-Al_2O_3 support and of the oxidic forms of the catalysts are presented in Fig. 2. Only 20% MoO_3 showed a peak at a *d*-spacing of 3.79 Å corresponding to crystalline MoO_3. Extra peaks also appeared for the bimetallic NiO–MoO_3 catalyst at 3.33 and 2.89 Å, which indicate the interaction between NiO and MoO_3.

Reaction Studies

The HDS, HDN, and simultaneous HDS/HDN results obtained at 400°C over 10% NiO, 20% MoO_3, and 3% NiO–15% MoO_3 are presented in Fig. 3. Thiophene HDS is significantly inhibited by the presence of pyridine in the gas phase, while pyridine HDN is enhanced by gas phase thiophene or H_2S over all three catalysts. The enhancement effect of thiophene or H_2S HDN, although visible on all three catalysts, is most pronounced over the

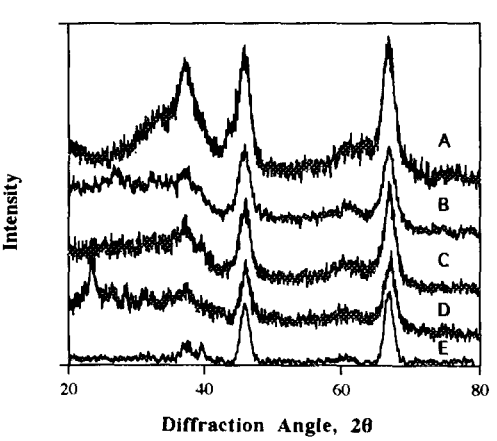

FIG. 2. X-ray diffraction patterns of (A) 10% NiO/γ-Al_2O_3, (B) 3% NiO–15% MoO_3/γ-Al_2O_3, (C) 15% MoO_3/γ-Al_2O_3, (D) 20% MoO_3/γ-Al_2O_3, and (E) γ-Al_2O_3.

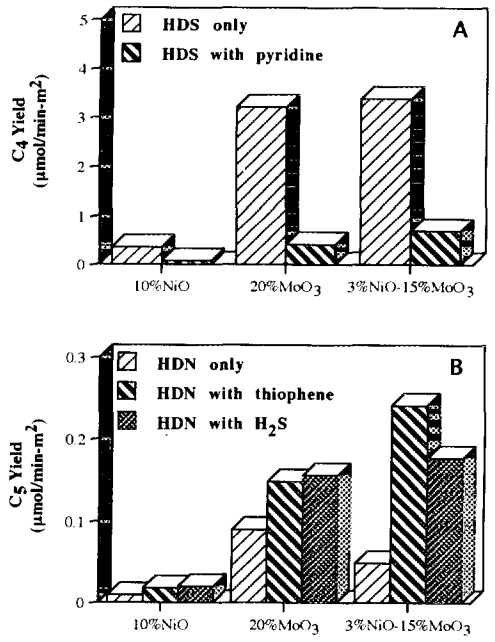

FIG. 3. (A) C_4 yield in thiophene HDS at 400°C and (B) C_5 yield in pyridine HDN at 400°C.

bimetallic catalyst. The presence of the nickel promoter in MoO_3 moderately increases the thiophene HDS rate in the absence of pyridine in the gas phase. The promoting effect of Ni on pyridine HDN is significant in the presence of thiophene or H_2S in the gas phase, but does not exist in the absence of sulfur compounds.

Figure 4 shows the effect of sulfur compounds on the individual steps of the HDN network by comparing the C_5 yield to the pyridine conversion. As reported in our earlier studies (18), the reaction pathway for pyridine HDN can be represented as a two-step sequence where pyridine is hydrogenated to piperidine, which, in turn, is converted to C_5 and ammonia through a hydrogenolysis process. In the presence of sulfur compounds, the C_5 yield is seen to be equal to the pyridine conversion rate. However, when there are no sulfur compounds present in the gas phase there are substantial levels of piperidine left in the system, making the pyridine conversion rates higher than the C_5 yields.

Figure 5 depicts the effect of thiophene on pyridine conversion rate at different temperatures. The presence of thiophene promoted the pyridine conversion over the bimetallic catalyst at all temperatures, especially at high temperatures (360, 400°C) where it increased HDN rate by 200–300%. However, it exhibited a dual effect over the monometallic Mo catalyst. At low temperatures (320°C), thiophene was seen to inhibit pyridine conversion by 40%, but at high temperatures (360, 400°C) there was a minor enhancement of about 10%. The details of the reaction study results have been presented elsewhere (18).

XPS Measurements

The X-ray photoelectron spectra of the pure γ-Al_2O_3 support were taken before and after being exposed to the same reaction environments (sulfidation, HDS, HDN, and simultaneous HDS/HDN) as the active catalysts. Under the high vacuum operating conditions of XPS measurement (10^{-9} Torr), sulfur was not detected after any of the treatments, indicating that there is no bonding between pure alumina and sulfur and that the sulfur exists only as part of the active catalyst phase.

Figure 6 shows the Ni 2*p* spectral region for the 10% NiO/γ-Al_2O_3 sample before and after sulfidation. Also displayed in Fig. 6 are the deconvolution results of the spectra by Gaussian–Lorentzian curve-fitting method. The same deconvolution procedure was used for all of the XPS spectra obtained in this study to determine binding

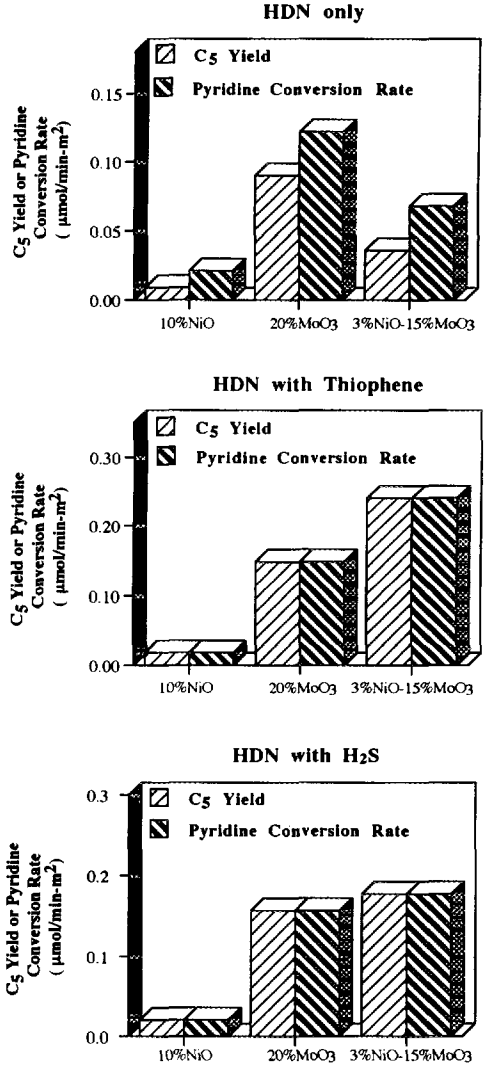

FIG. 4. C_5 yields and pyridine conversion rates in HDN alone, HDN with thiophene, and HDN with H_2S.

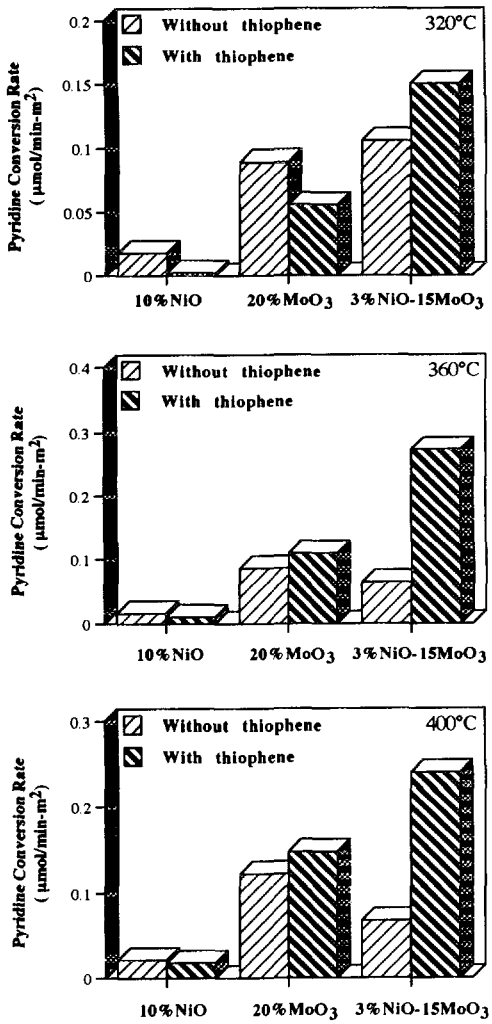

FIG. 5. Pyridine conversion rate in the presence and absence of thiophene at different temperatures.

energies and peak areas. The Ni $2p_{3/2}$ binding energy for the oxidic sample was 856.1 eV, with a strong shake-up satellite at ca. 862 eV. For the sulfided sample, the peak at 856.1 eV persisted although the intensity of the shake-up line at ca. 862.0 eV after sulfiding was much lower, and a new feature appeared at 852.8 eV, corresponding to nickel in the sulfided form. The area ratio of the peaks at 852.8 and 856.1 eV was about 0.5, indicating that a considerable portion of Ni in this catalyst could not be sulfided or reduced. A similar result was reported by Grimblot et al. (32) for sulfided 3% NiO/γ-Al_2O_3 catalyst. According to Ng and Hercules (33) and Huang and Schwarz (34), this portion of Ni is in the form of $NiAl_2O_4$. They also found that the nickel aluminate has the same XPS peak position with nickel oxide; however, the differentiation between the two Ni species can be achieved after sulfiding since the latter can be easily sulfided whereas the former cannot.

From Fig. 7, which compares the Ni 2*p* spectral region for the 10% NiO catalyst after different treatments, it is seen that all of the postreaction spectra of the sample were similar to that of the oxide form of the catalyst, although they now had a feature corresponding to the sulfide. The intensity of the $NiAl_2O_4$ signal and the shake-up line increased significantly at the expense of the sulfided nickel signal intensity (peak at 852.8 eV).

The Ni 2*p* XPS spectra of the 10% NiO and 3% NiO–15% MoO_3 samples before and after sulfidation are compared in Fig. 8. The two samples showed similar spectra before sulfiding, indicating that Ni in the oxide phase of the monometallic Ni and bimetallic Ni–Mo catalysts existed in the same form. The Ni 2*p* spectra for the sulfided Ni and Ni–Mo samples, on the other hand, showed a significant difference. Unlike in the single metal nickel catalyst, the peak corresponding to $NiAl_2O_4$ species almost disappeared for the bimetallic Ni–Mo catalyst. A Ni $2p_{3/2}$ binding energy of 853.0 eV was obtained for the Ni–Mo catalyst, implying that Ni in the sulfided Ni–Mo catalyst existed mainly in a single phase.

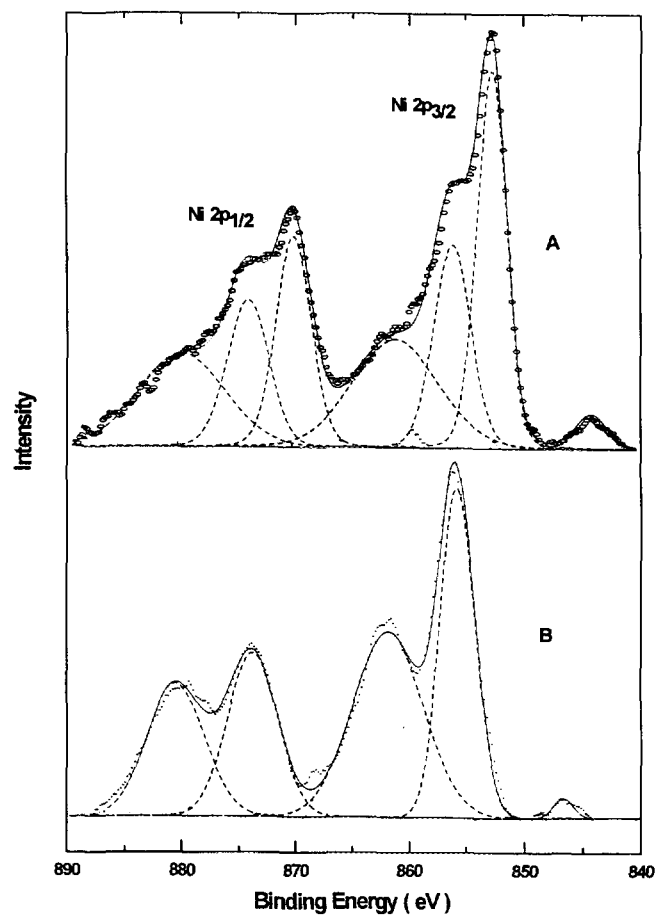

FIG. 6. XPS spectra of Ni 2*p* region and deconvolution results for sulfided 10% NiO/γ-Al_2O_3 (A) after sulfidation and (B) before sulfidation.

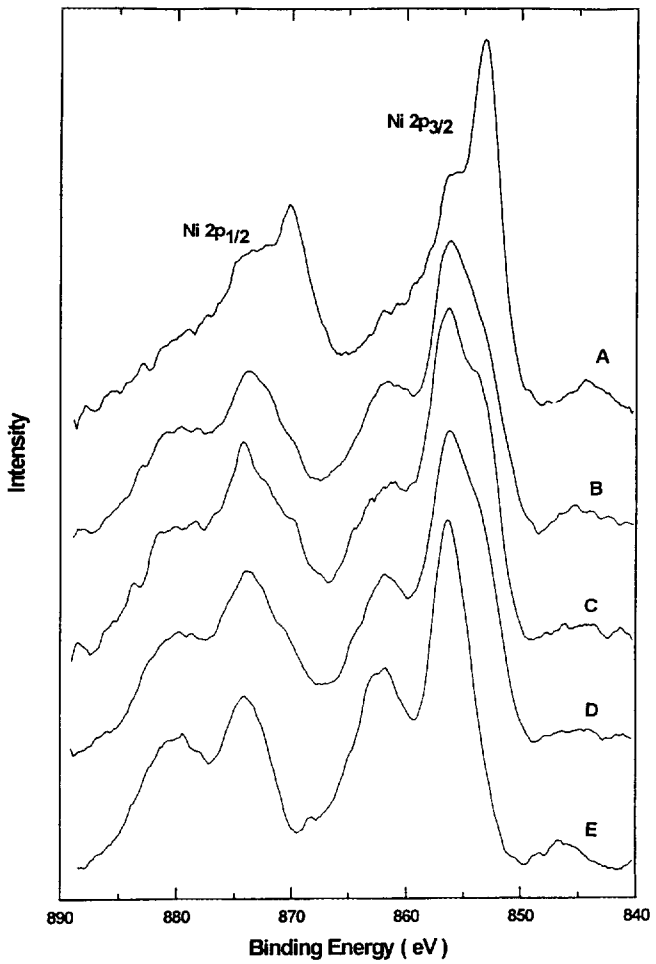

FIG. 7. XPS spectra of 10% NiO/γ-Al_2O_3 in Ni 2*p* region (A) after sulfidation, (B) after thiophene HDS, (C) after simultaneous thiophene HDS and pyridine HDN, (D) after pyridine HDN, and (E) before sulfidation.

Figure 9 shows the postreaction Ni 2*p* XPS spectra of the sulfided 3% NiO–15% MoO_3 catalyst. This figure, unlike Fig. 7, shows no major change in the Ni 2*p* spectra with the reaction environment, suggesting that the reaction environment had little effect on the structure of Ni species in the sulfided bimetallic Ni–Mo catalyst.

The XPS spectra of the Mo 3*d*–S 2*s* region for the 20% MoO_3 catalyst following different treatments are presented in Fig. 10. After sulfidation, the binding energy for Mo $3d_{5/2}$ decreased from 232.8 to 228.8 eV, corresponding to the change from MoO_3 to MoS_2. The spectra taken after different reactions, however, remained almost identical. In Fig. 11, the Mo 3*d* spectrum of the bimetallic Ni–Mo catalyst before sulfidation is compared with that of the monometallic Mo catalyst. The results show no noticeable difference between the spectra of the two catalysts in the oxide form.

Figure 12 presents the Mo 3*d*–S 2*s* spectral region and the curve fitting results for sulfided forms of both mono- and bimetallic catalysts after simultaneous HDS/HDN reactions. It should be noted that a complete deconvolution of the Mo 3*d* doublet was not attempted here. The similarity between the Mo 3*d* spectra of the mono- and bimetallic catalysts as shown in Figs. 11 and 12 suggested that Mo in the two catalysts had a similar coordination environment. Although no apparent difference for the Mo 3*d* peaks between the two samples was observed, the S 2*s* signal for the bimetallic catalyst was seen to be significantly stronger than that for the monometallic Mo catalyst. This fact is an indication that the Ni–Mo catalyst had a higher sulfur content than the Mo catalyst at the steady-state HDS/HDN reaction conditions. The postreaction Mo 3*d*–S 2*s* spectra for the sulfided 3% NiO–15% MoO_3 catalyst are shown in Fig. 13. Again, the Mo 3*d* spectra showed no observable difference after different treatments.

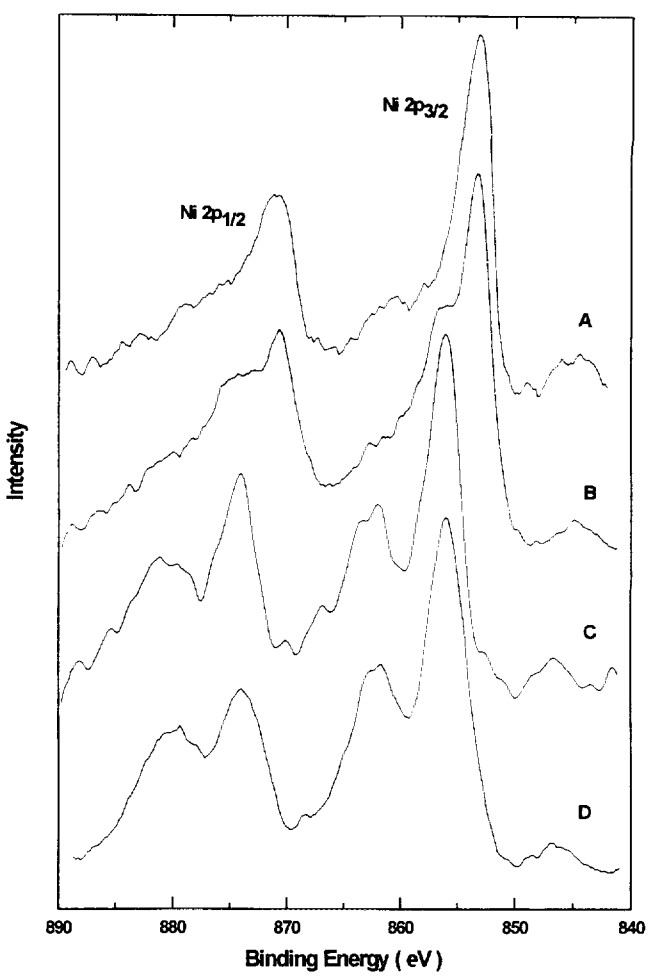

FIG. 8. Comparison of Ni 2*p* XPS spectra for 10% NiO/γ-Al_2O_3 and 3% NiO–15% MoO_3/γ-Al_2O_3 catalysts. (A) 3% NiO–15% MoO_3/γ-Al_2O_3 after sulfidation, (B) 10% NiO/γ-Al_2O_3 after sulfidation, (C) 3% NiO–15% MoO_3/γ-Al_2O_3 before sulfidation, and (D) 10% NiO/γ-Al_2O_3 before sulfidation.

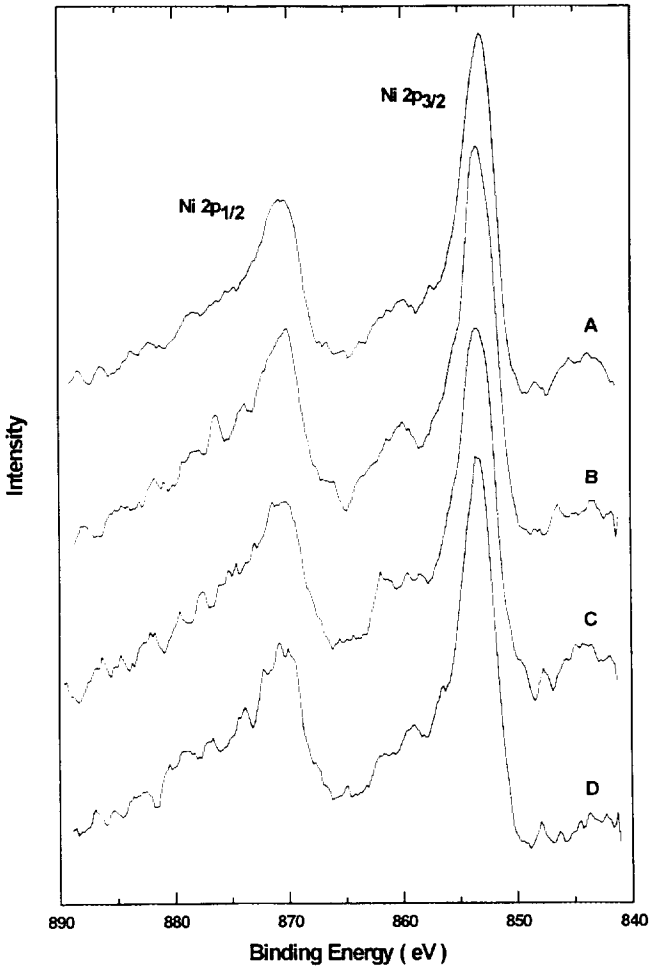

FIG. 9. XPS spectra of Ni 2*p* region for 3% NiO–15% MoO_3/-Al_2O_3 (A) after sulfidation, (B) after thiophene HDS, (C) after simultaneous thiophene HDS and pyridine HDN, and (D) after pyridine HDN.

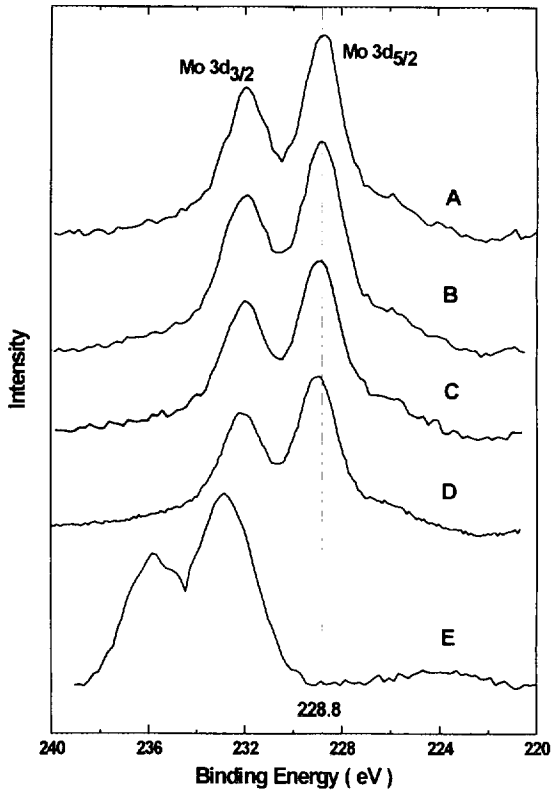

FIG. 10. XPS Spectra of Mo 3*d* Region for 20% MoO_3/γ-Al_2O_3 (A) after sulfidation, (B) after thiophene HDS, (C) after simultaneous thiophene HDS and pyridine HDN, (D) after pyridine HDN, and (E) before sulfidation.

Binding energies of S 2*p* were determined for the single metal Ni, Mo, and bimetallic Ni–Mo catalysts at various conditions. The value of S 2*p* was in the range of 162.1 ± 0.2 eV for all the samples. Table 1 summarizes the binding energies of S 2*p*, Ni $2p_{3/2}$, Mo $3d_{5/2}$, and the Δ BEs between Ni, Mo, and S obtained in this work. The binding energies of S 2*p* and Mo 3*d* reported here are in agreement with those reported earlier in the literature for Mo and Co- or Ni-promoted Mo catalysts (24–26, 35–37). Since the available data for Ni 2*p* binding energy on similar catalyst systems in the literature are very limited, a comparison is more difficult to make. However, the values obtained in this study seem to be consistent with the trend in the literature values for both Co- and Ni-promoted Mo catalysts that the binding energy for the promoter ion is higher in the bimetallic catalysts than in its bulk sulfide (24–26), and this trend can be explained by the higher Ni–S coordination number in the bimetallic system than in the bulk nickel sulfide (38).

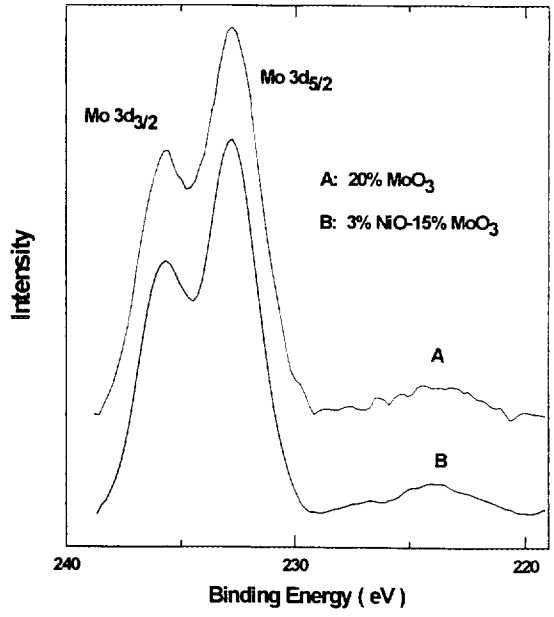

FIG. 11. Comparison of XPS spectra of Mo 3*d* region for oxide forms of 20% MoO_3/γ-Al_2O_3 and 3% NiO–15% MoO_3/γ-Al_2O_3.

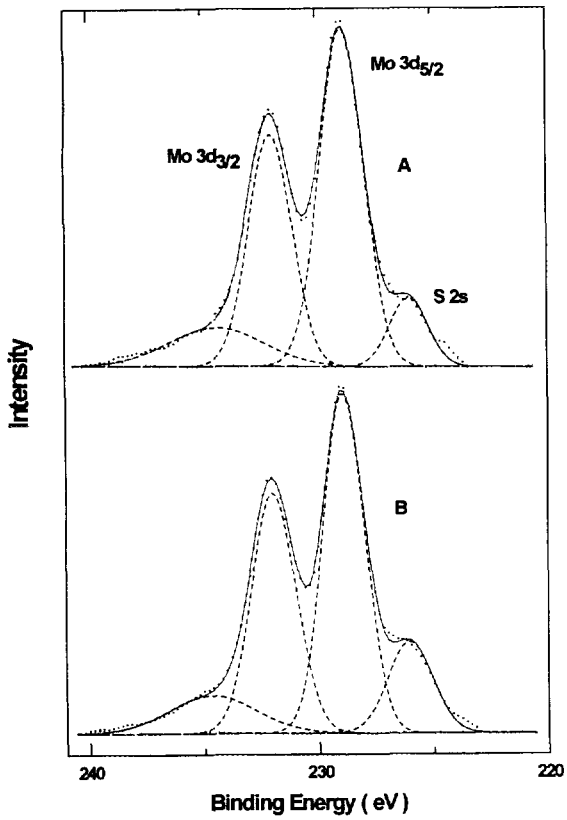

FIG. 12. Comparison of XPS spectra of Mo $3d$–S $2s$ region for 20% MoO_3/γ-Al_2O_3 and 3% NiO–15% MoO_3/γ-Al_2O_3 after simultaneous HDS/HDN including curve fitting results.

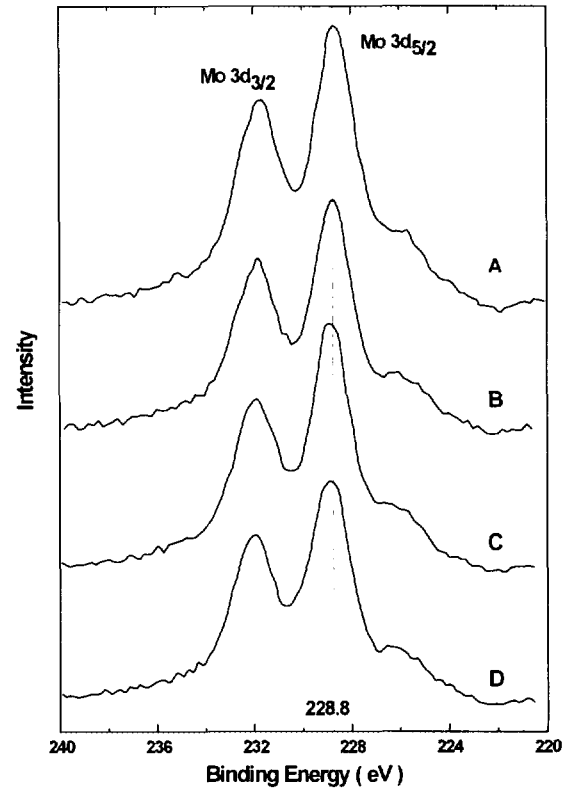

FIG. 13. XPS spectra of Mo $3d$–S $2s$ region for 3% NiO–15% MoO_3/γ-Al_2O_3 (A) after sulfiding, (B) after thiophene HDS, (C) after simultaneous thiophene HDS and pyridine HDN, and (D) after pyridine HDN.

TABLE 1

XPS Binding Energy Shift after Different Reactions (eV)

	Catalyst	Untreated	H_2S	HDS	HDS/HDN	HDN
Ni $2p_{3/2}$	10% NiO	856.1	852.8	853.0	853.1	853.0
	3% NiO–15% MoO_3	856.2	853.0	853.4	853.4	853.3
Mo $3d_{5/2}$	20% MoO_3	232.8	228.7	228.8	228.9	228.9
	3% NiO–15% MoO_3	232.8	228.7	228.8	228.9	228.9
S $2p$	10% NiO	—	162.0	162.2	162.3	162.2
	20% MoO_3	—	162.0	162.1	162.1	162.3
	3% NiO–15% MoO_3	—	162.0	162.1	162.1	162.2
ΔB.E. (Ni $2p_{3/2}$–S $2p$)	10% NiO	—	690.8	690.8	690.8	690.8
	3% NiO–15% MoO_3	—	691.0	691.4	691.3	691.1
ΔB.E. (Mo $3d_{5/2}$–S $2p$)	20% MoO_3	—	66.7	66.6	66.7	66.6
	3% NiO–15% MoO_3	—	66.6	66.7	66.7	66.7

XPS results can be quantified either by intensity or by peak area for obtaining relative surface concentrations. In this study, XPS peak area ratios were used since they better reflect the quantitative relation to the composition. The ratio of peak areas $A_{Mo\ 3d}/A_{Al\ 2p}$ is usually used to illustrate the dispersion of Mo on the support. It is suggested that at low Mo loadings, $A_{Mo\ 3d}/A_{Al\ 2p}$ is proportional to the Mo/Al atomic ratio (39). Figures 14a and 14b show the ratios of $A_{Mo\ 3d}/A_{Al\ 2p}$ and $A_{Ni\ 2p}/A_{Al\ 2p}$ for both mono- and bimetallic catalysts. For the monometallic Mo or Ni catalyst, no obvious difference in this ratio was found between the fresh and the used catalysts. This result suggests that sulfidation and different reaction media do not affect the dispersion of monometallic Mo or Ni on alumina surface significantly. For the bimetallic Ni–Mo catalyst, however, significant increase of $A_{Mo\ 3d}/A_{Al\ 2p}$ and $A_{Ni\ 2p}/A_{Al\ 2p}$ ratios was seen after sulfidation, implying that the dispersion of both Mo and Ni on γ-Al_2O_3 is greatly improved by sulfidation. The area ratios essentially remained unchanged after the catalysts were used in different reaction media (HDS, HDN, HDS/HDN), suggesting that the dispersion remained unaffected by the reactions. Figure 14c shows the ratios of $A_{S\ 2p}/A_{Al\ 2p}$. A higher $A_{S\ 2p}/A_{Al\ 2p}$ was seen for bimetallic Ni–Mo catalyst than for monometallic Mo catalyst or monometallic Ni catalyst.

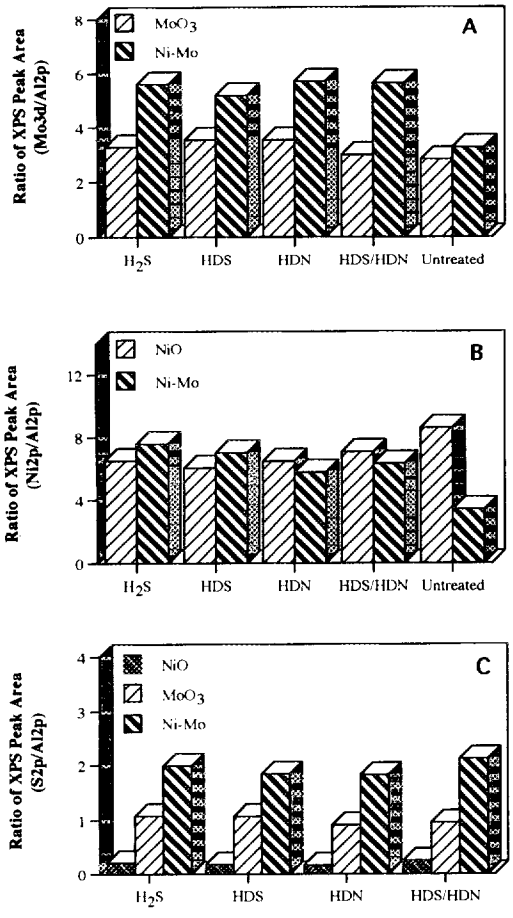

FIG. 14. Variation of XPS peak area ratios with the reaction medium. (A) Mo 3*d*/Al 2*p*, (B) Ni 2*p*/Al 2*p*, and (C) S 2*p*/Al 2p.

Although the difference between the bimetallic catalyst and the monometallic Ni catalyst can be attributed to the difference in loading levels (10% NiO vs 3% NiO–15% MoO_3), the difference between the bimetallic catalyst and monometallic Mo catalyst (3% NiO–15% MoO_3 vs 20% MoO_3) suggests either a higher sulfur content or a higher dispersion over the Ni–Mo/γ-Al_2O_3 catalyst.

The ratio of $A_{S\ 2p}/A_{Mo\ 3d}$ presented in Fig. 15 provides a measure of the degree of sulfidation. The results show that after HDN reaction in the absence of thiophene or H_2S in the gas phase, $A_{S\ 2p}/A_{Mo\ 3d}$ decreased noticeably for both Mo and Ni–Mo catalysts, indicating a decrease in sulfur content on the surface. It should also be noted that the combined HDS/HDN reaction leaves the surface in a more sulfided state than does HDS reaction alone and that the reaction medium (HDS/HDN) which leaves the bimetallic catalyst in the most sulfided form also leads to the highest HDN activity, as seen in Fig. 3.

Temperature-Programmed Desorption

Figure 16 presents the H_2S TPD profiles over the γ-Al_2O_3 support, 10% NiO, 20% MoO_3, and 3% NiO–15% MoO_3 catalysts after sulfidation. The loading was 200 mg for each sample. There are two major desorption peaks for each sample, with the first temperature maximum, which corresponds to physisorbed H_2S, appearing at 70°C for all samples. The maximum of the second H_2S desorption peak was at 472, 482, and 490°C for the monometallic Ni and Mo, and bimetallic Ni–Mo catalysts, respectively. The γ-Al_2O_3 support, however, showed a much lower desorption temperature at 200°C for the second H_2S peak, indicating that no adsorbed H_2S was present on the surface at reaction conditions. Another feature to note is a small shoulderlike feature at 605°C on the TPD profile of the bimetallic catalyst, which was seen in neither Ni- or Mo monometallic catalyst. This could imply the existence of Ni–Mo interaction sites which bind H_2S more strongly than monometallic sites.

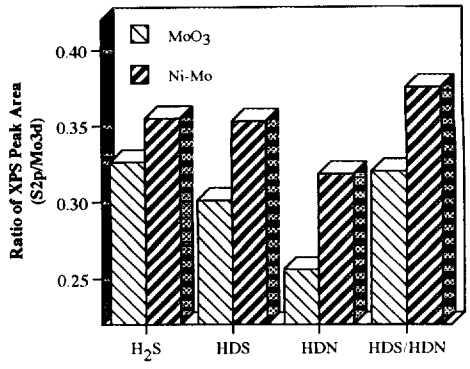

FIG. 15. Effect of the presence of sulfur compounds on pre- and postreaction XPS peak area ratio of S 2*p*/Mo 3*d* for 20% MoO_3/γ-Al_2O_3 and 3% NiO–15% MoO_3/γ-Al_2O_3.

Postreaction TPD results showed that the amount of thiophene desorbed from the bimetallic catalyst was larger

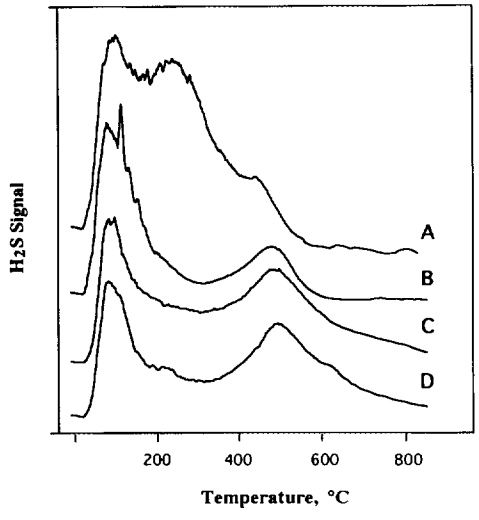

FIG. 16. H_2S TPD profiles of sulfided samples. (A) Pure γ-Al_2O_3, (B) 10% NiO/γ-Al_2O_3, (C) 20% MoO_3/γ-Al_2O_3, and (D) 3% NiO–15% MoO_3/γ-Al_2O_3.

than that desorbed from the monometallic Mo catalyst after both HDS and HDS/HDN reactions. Pyridine desorption over the monometallic Mo catalyst was higher after HDN alone than after HDS/HDN, whereas the opposite was true over the bimetallic Ni–Mo catalyst. This result suggests that the role of thiophene in HDN is somewhat different over the mono- and bimetallic catalysts.

DISCUSSION

As described in the Results section, XPS measurements showed that the binding energies of Mo $3d_{5/2}$ and S $2p$ were about the same for the sulfided forms of both monometallic Mo and bimetallic Ni–Mo catalysts. This suggests that the Mo and S phase structure in the Ni–Mo catalyst is the same as it is in the monometallic Mo catalyst. The binding energy of Ni $2p_{3/2}$ and the Ni $2p$ spectra, however, showed significant differences between the bi- and monometallic catalysts, especially after being used in different reaction media, suggesting that nickel in the sulfided Ni–Mo catalyst exists in a different coordination environment than it does in the sulfided monometallic Ni catalyst. Although further characterization is needed for conclusive determination of the phase structure, the Ni–Mo–S model proposed by Topsøe and co-workers (3, 21, 22) appears to be the most likely phase structure for the bimetallic catalysts used in this study.

It has been reported that when the loading is below ca. 4–5 Mo atoms/nm^2, the Mo atoms will be highly dispersed on the support as a monolayer (40, 41). As the Mo loading increases, the structure of Mo oxide changes from a highly dispersed state to a three-dimensional multilayer morphology. For the 20% MoO_3 catalyst in our experiment, the Mo loading (ca 5.7 atoms/nm^2) was higher than a monolayer, and for the 15% MoO_3 catalyst the Mo loading (ca. 4.5 atoms/nm^2) was around a monolayer. However, the LRS results in Fig. 1 show that, for the monometallic MoO_3 catalyst, crystalline MoO_3 was found at a Mo loading level of 15 wt% or higher. This fact implies that the oxidic monometallic Mo catalysts prepared in these studies were not completely dispersed over the γ-Al_2O_3 support.

LRS results in Fig. 1 show that the crystalline MoO_3 which was detected in 15% MoO_3 did not appear in 3% NiO–15% MoO_3. XPS peak area ratios $A_{Mo\ 3d}/A_{Al\ 2p}$ (Fig. 14a), which are indicative of the degree of Mo dispersion, also show 3% NiO–15% MoO_3 to have a higher dispersion than 20% MoO_3. These observations lead us to suggest that one of the roles of the Ni promoter is to improve the dispersion of Mo over the γ-Al_2O_3 support, which is in agreement with the conclusion obtained by Ledoux *et al.* (23).

XPS area ratios in Fig. 14a show that bimetallic Ni–Mo catalyst had a large increase in $A_{Mo\ 3d}/A_{Al\ 2p}$ after sulfidation, indicating sulfided Ni–Mo attained a much higher Mo dispersion level than its oxide form. These results show that, although adding Ni to Mo alone can improve the dispersion of Mo, the improvement becomes more substantial after sulfidation. In Fig. 14a it is also seen that there was a slight increase of $A_{Mo\ 3d}/A_{Al\ 2p}$ for the single-metal Mo catalyst after sulfidation, indicating that in the absence of Ni, sulfidation may only improve the dispersion of Mo slightly. Based on these results, it is conceivable that the apparent increase in the dispersion of the Ni–Mo catalyst after the sulfidation step may be due to formation of the Ni–Mo–S structure.

In our reaction studies (18), the HDN of pyridine was found to undergo two main successive steps as suggested by McIlvried (7). In the first step, pyridine is hydrogenated to form piperidine, and in the second step, hydrogenolysis of piperidine through C–N bond cleavage takes place to form C_5 and ammonia. The findings in our reaction and characterization studies, along the lines of some of the earlier postulates in the literature (10), suggest the existence of two major types of active sites promoting HDN of pyridine. Type I: these are pyridine hydrogenation sites consisting of sulfur vacancies associated with Mo (type Ia sites) or Ni in Ni–Mo–S (type Ib sites). Type II: these are piperidine hydrogenolysis sites consisting of Brønsted acid centers associated with Mo atoms only.

The role of type Ia sites (sulfur vacancies associated with Mo atoms) has been recognized as promoting hydrogenation of pyridine and was initially proposed by Satterfield *et al.* (9). The presence of type Ib sites (sulfur vacancies associated with Ni atoms in Ni–Mo–S phase) has been found by Topsøe and co-workers (3, 22) and confirmed by other researchers, including Louwers and Prins (38). However, the role of type Ib sites in HDN reactions is not well understood. Perot *et al.* (17) concluded that vacancies involving Ni catalyze hydrogenation. Our reaction results (18) were in agreement with this conclusion, showing that when the rate determining step is the hydrogenation of pyridine, the Ni promoter significantly increases the HDN rate, but when hydrogenolysis is rate determining, the Ni has no promotional effect. Considering the anion vacancy nature of the Ni-promoted active sites (42), a role similar to that played by sulfur vacancies associated with Mo in promoting hydrogenation of pyridine seems plausible for Ni in the Ni–Mo–S structure. Sulfur vacancies are preferentially formed in those edge and corner Ni or Mo sites, where chemically unsaturated sulfur atoms are located. These sulfur atoms, in turn, react with hydrogen to form H_2S, leaving sulfur vacancies behind.

Although both types of S vacancies are thought to promote hydrogenation of pyridine, the rate over S vacancies associated with Ni in Ni–Mo–S appears to be much higher than the rate over those associated with Mo. This is analogous to the thiophene HDS case where the Ni-promoted

site has a much higher intrinsic HDS activity than unpromoted sites (3). It is shown by our reaction studies results (Figs. 3 and 5) that, where hydrogenation is the rate-determining step, much higher pyridine conversion rates were seen over Ni–Mo than over the monometallic Mo catalyst in the presence of sulfur compounds. However, the much lower enhancement effect of sulfur compounds on HDN over the monometallic Mo catalyst seems to be caused not only by the lower intrinsic activity of sulfur vacancies associated with Mo, but also by the decreased number of these sites in the presence of sulfur compounds.

Type II sites are Brønsted acid sites (H^+) associated with Mo atoms. These have been found to be responsible for hydrogenolysis. According to Yang and Satterfield (10), the adsorption and dissociation of an H_2S molecule can convert a sulfur vacancy to a Brønsted acid site and a sulfhydryl group (SH), but the adsorption is readily reversible if H_2S is removed from the reaction system. The presence of type II sites under reaction conditions was demonstrated by Burch and Collins in a TPD study of sulfided Ni–Mo/Al_2O_3 hydrotreating catalysts (43) and was further confirmed by Topsøe *et al.* (44) in infrared studies of pyridine adsorption over Ni–Mo and Co–Mo catalysts supported on alumina. Moreover, both studies suggested that Brønsted acid sites (H^+) were associated only with Mo and not with the promoter atoms.

In our reaction studies, a strong dependence of the hydrogenolysis rate on gas phase sulfur compounds was observed (Fig. 4) which seems to reflect the strong dependence of the Brønsted acid sites on the presence of H_2S. In addition, our postreaction XPS results in Fig. 15 showed a pronounced decrease in area ratio of $A_{S\,2p}/A_{Mo\,3d}$ over both monometallic and bimetallic catalysts after being used in HDN reaction. This implies that the low HDN rate in the absence of gas phase sulfur corresponds to the low degree of sulfidation in these catalysts. Our H_2S TPD results in Fig. 16 showed a broad H_2S desorption peak in the 350–600°C range from the MoS_2 phase of both single-metal Mo and Ni–Mo catalysts. As proposed by other researchers (9, 10, 13), these desorbed H_2S molecules are very likely to be desorbed from the Brønsted acid sites and their associated SH groups.

As reported previously, in our reaction studies the addition of Ni to Mo showed no promotion effect on the hydrogenolysis step (18). This can also be seen in Fig. 3, which shows that when hydrogenolysis is the rate-determining step (at high temperatures and in the absence of gas phase sulfur compounds) 20% MoO_3 had a higher HDN rate than 3% NiO–15% MoO_3 catalyst. Supposing that Brønsted acid sites are not associated with Ni, the higher HDN activity over 20% MoO_3 would be linked to a higher content of Brønsted acid sites. Therefore, it could be suggested that Brønsted acid sites are indeed only associated with Mo atoms. The fact that, in our H_2S TPD experiments, the amount of H_2S desorbing from 20% MoO_3 was 10% more than that desorbing from 3% NiO–15% MoO_3 catalyst seems to be in agreement with this suggestion. Also supporting this argument is the finding of Hanlon (11), who reported that pyridine hydrogenation rate over a sulfided commercial Ni–Mo/Al_2O_3 catalyst was unaffected by the partial pressure of H_2S. This finding can be explained by our proposed catalytic job distribution in which hydrogenation of pyridine is mainly carried out on Ni-associated S vacancies, which, unlike Mo-associated S vacancies that can easily be converted into Brønsted acid sites by H_2S in the gas phase, are hardly affected by H_2S.

In Fig. 5a we see an inhibition effect of thiophene on pyridine conversion rate over the monometallic Mo catalyst and an enhancement effect over the Ni–Mo catalyst at low temperature where hydrogenation is the rate-determining step. The inhibition effect of thiophene over the monometallic Mo catalyst can be explained by the decrease in the available hydrogenation sites on the catalyst through H_2S molecules (the product of thiophene HDS) which readily convert the sulfur vacancies into Brønsted acid sites, and by the competitive adsorption between pyridine and thiophene on these sites. The role of thiophene over Ni–Mo catalyst appears to be somewhat different, however, since in our reaction conditions the presence of thiophene was always seen to enhance the HDN activity.

Topsøe *et al.* used nitrosylated inorganic clusters to better understand the structural and electronic environment of the Co-edge promoter atoms in Co–Mo/Al_2O_3 HDS catalysts (45). Using NO as a probe molecule in adsorption experiments, they found that the promotion of the catalytic activity was related to the number of Co atoms that can bind NO. They concluded that, since NO is not expected to replace S at the adsorption temperature, the promotion must involve Co-edge sites with substantial coordinative unsaturation (i.e., sulfur vacancies). They also indicated that there are two S vacancies in a Co-edge site which can be occupied by two NO molecules. Ledoux and Djellouli (12) proposed that there might be some metallic nickel atoms with zero valence on the surface of Ni–Mo bimetallic catalysts. Topsøe and Clausen also indicated a Ni–S coordination number lower than that for Mo–S and the possible existence of double vacancies associated with the promoter atoms (42). Through a hydrogenation study for some large nitrogen compounds over sulfided Ni–Mo and other catalysts, Shabtai *et al.* (46) suggested that there are at least three possible double sulfur vacancy sites over such catalyst systems, i.e., edge, corner, and valley double vacancies. These findings in the literature combined with our experimental data lead us to suggest that double vacancies associated with Ni atoms can exist under reaction conditions and that these

double vacancies can be poisoned by piperidine molecules which lead to a reduction of the available number of active sites for pyridine hydrogenation.

The poisoning effect of piperidine on double vacancy sites can possibly be explained by the fact that piperidine has a stronger basic property than other molecules in the pyridine HDN system and tends to bind to the site more strongly. Also, the larger adsorption area available in a double vacancy site makes it more prone to poisoning by piperidine, which has a larger molecular size than pyridine. The enhancement effect of thiophene on the pyridine hydrogenation step could, therefore, be due to the conversion of double sulfur vacancies into single vacancies by thiophene. When one considers the high intrinsic HDS activity of the Ni-associates sulfur vacancies and the HDS mechanism that involves direct extrusion of sulfur from thiophene (13), one would expect the conversion of double sulfur vacancies to single vacancies by thiophene to be a likely step. It is conceivable that the single vacancies are not as prone to poisoning by piperidine as double vacancies are, and hence the pyridine hydrogenation activity over Ni sites remains high in the presence of thiophene.

As seen in Fig. 3b, HDN activity for the Ni–Mo catalyst in the presence of 0.87% thiophene was significantly higher than in the presence of 0.87% H_2S. This can be explained by the adsorption affinity of thiophene on the double sulfur vacancies which is much higher than that of H_2S. Shabtai *et al.* (46) pointed out that H_2S either does not adsorb at all or adsorbs weakly on the edge or corner double vacancies. Indirect evidence for the preferential filling of double vacancies by thiophene compared to H_2S on the bimetallic Ni–Mo catalyst is shown in Fig. 15. The higher sulfur content of the catalyst after simultaneous HDN/HDS reaction than after thiophene HDS alone was demonstrated by the higher XPS area ratios of $A_{S\,2p}/A_{Mo\,3d}$ in the HDN/HDS case. Since thiophene HDS is inhibited by nitrogen compounds (Fig. 3a), thiophene concentration in the gas phase is higher in sumultaneous HDN/HDS than in HDS alone. Conversely, H_2S concentration in the gas phase is higher for thiophene HDS alone since it is the reaction product and the reaction nearly goes to completion. Therefore, thiophene appears to be much more efficient than H_2S in helping to maintain a higher concentration level of Ni-associated single sulfur vacancies and, hence, a higher pyridine hydrogenation activity over bimetallic catalysts.

Similar studies performed over the unsupported Ni, Mo, and Ni–Mo sulfide catalysts suggested the presence of a job distribution between Ni and Mo sites over these catalysts similar to that found over the supported catalysts. The findings obtained over the unsupported model Ni–Mo sulfide catalysts and the comparison of those findings to the phenomena observed over the supported catalysts are reported in the next paper in this series (47).

SUMMARY

From the discussions above, the role of Ni in HDN of pyridine can be summarized as follows: (1) It enhances the dispersion of Mo over the γ-Al_2O_3 support. This enhancement is particularly substantial after sulfiding due to the formation of the "Ni–Mo–S" structure. (2) It promotes the hydrogenation of pyridine through the synergistic active sites (type Ib sites) which are single sulfur vacancies associated with Ni in Ni–Mo–S structure.

The role of sulfur compounds in HDN catalytic scheme was also found to be multifaceted: (1) H_2S in the gas phase helps maintain a certain content of Brønsted acid sites (type II sites), which are associated with Mo and promote the hydrogenolysis of piperidine. Thiophene promotes hydrogenolysis of piperidine indirectly via H_2S formed during HDS reaction. (2) Thiophene in the gas phase also helps the pyridine hydrogenation step over the bimetallic Ni–Mo catalysts by keeping Ni-active sites in an effective form (by converting double S vacancies to single vacancies) for pyridine hydrogenation reaction. (3) Thiophene in the gas phase does not enhance the hydrogenation step over the monometallic Mo catalyst, but inhibits it by reducing the number of available hydrogenation sites.

ACKNOWLEDGMENTS

Financial support provided by the National Science Foundation through Grant EID-9023778 and by the Exxon Corporation is gratefully acknowledged. The authors also thank Mr. Paul A. Clark for his help in the preparation of the manuscript.

REFERENCES

1. Schuit, G. C. A., and Gates, B. C., *AIChE J.* **19,** 417 (1973).
2. Grange, P., *Catal. Rev.—Sci. Eng.* **21,** 135 (1980).
3. Topsøe, H., and Clausen, B. S., *Catal. Rev.—Sci. Eng.* **26,** 395 (1984).
4. Prins, R., de Beer, V. H. J., and Somorjai, G. A., *Catal. Rev.—Sci. Eng.* **31,** 1 (1989).
5. Ho, T. C., *Catal. Rev.—Sci. Eng.* **30,** 117 (1988).
6. Girgis, M. J., and Gates, B. C., *Ind. Eng. Chem. Res.* **30,** 2021 (1991).
7. McIlvried, H. G., *Ind. Eng. Chem. Process Des. Dev.* **10,** 125 (1971).
8. Satterfield, C. N., Modell, M., and Mayer, J. F., *AIChE J.* **21,** 1100 (1975).
9. Satterfield, C. N., Modell, M., and Wilkens, A., *Ind. Eng. Chem. Process. Des. Dev.* **19,** 154 (1980).
10. Yang, S. H., and Satterfield, C. N., *J. Catal.* **81,** 168 (1983).
11. Hanlon, R. T., *Energy Fuels* **1,** 424 (1987).
12. Ledoux, M. J., and Djellouli, B., *Appl. Catal.* **67,** 81 (1990).
13. Hadjiloizou, G. C., Butt, J. B., and Dranoff, J. S., *Ind. Eng. Chem. Res.* **31,** 2503 (1992).

14. Hadjiloizou, G. C., Butt, J. B., and Dranoff, J. S., *J. Catal.* **135,** 27 (1992).
15. Tischer, R. E., Narain, N. K., Stiegel, G. J., and Cillo, D. L., *Prepr.—Am. Chem. Soc., Div. Pet. Chem.* **30,** 459 (1985).
16. Olalde, A., and Perot, G., *App. Catal.* **13,** 373 (1985).
17. Perot, G., Brunet, S., and Hamze, N., *in* "Proceedings, 9th International Congress on Catalysis, Calgary, 1988" (M. J. Phillips and M. Ternan, Eds.), Vol. 1, p. 19. Chem. Institute of Canada, Ottawa, 1988.
18. Ozkan, U. S., Ni, S., Zhang, L., and Moctezuma, E., *Energy Fuels* **8,** 249 (1994).
19. Laine, R. M., *Catal. Rev.—Sci. Eng.* **25,** 459 (1983).
20. Nelson, N., and Levy, R. B., *J. Catal.* **58,** 485 (1979).
21. Topsøe, H., Clausen, B. S., Candia, R., Wivel, C., and Morup, S., *J. Catal.* **68,** 433 (1981).
22. Topsøe, N.-Y., and Topsøe, H., *J. Catal.* **84,** 386 (1983).
23. Ledoux, M., J., Maire, G., Hantzer, S., and Michaux, O., *in* "Proceedings, 9th International Congress on Catalysis, Calgary, 1988" (M. J. Phillips and M. Ternan, Eds.), Vol. 1, p. 74. Chem. Institute of Canada, Ottawa, 1988.
24. Alstrup, I., Chorkendorff, I., Candia, R., Clausen, B. S., and Topsøe, H., *J. Catal.* **77,** 397 (1982).
25. Shepelin, P., Zhdan, P. A., Burmistrov, V. A., Startsev, A. N., and Yermakov, Y. I. *Appl. Catal.* **11,** 29 (1984).
26. Blanchard, L., Grimblot, J., and Bonnelle, J. P., *J. Catal.* **98,** 229 (1986).
27. Radchenko, E. D., Landau, M. V., Nefedov, B. K., Nikulina, L. I., Chukin, G. D., Zhdan, P. A., Agievsky, D. A., and Sinkin, A. A., *in* "Proceedings, 8th International Congress on Catalysis, Berlin, 1984," Vol. 2, p. 399. Dechema, Frankfurt-am-Main, 1984.
28. Ozkan, U. S., Cai, Y., Kumthekar, M. W., and Zhang, L., *J. Catal.* **142,** 182 (1993).
29. Wang, L., and Hall, W. K., *J. Catal.* **66,** 251 (1980).
30. Chan, S. S., *J. Phys. Chem.* **88,** 5831 (1984).
31. Payen, E., *Appl. Spectrosc.* **36,** 30 (1982).
32. Grimblot, J., Dufresne, P., Gengembre, L., and Bonnelle, J., *Bull. Soc. Chim. Belg.* **90,** 1261 (1981).
33. Ng, K. T., and Hercules, D. M., *J. Phys. Chem.* **80,** 2094 (1976).
34. Huang, Y.-J., and Schwarz, J. A., *Appl. Catal.* **36,** 163 (1988).
35. Patterson, T. A., Carver, J. C., Leyden, D. E., and Hercules, D. M., *J. Phys. Chem.* **80,** 1700 (1976).
36. Sarbak, Z., and Andersson, L. T., *Appl. Catal.* **69,** 235 (1991).
37. Zaikovskii, V. I., Shepelin, P., Burmistrov, V. A., Startsev, A. N., and Yermakov, Y. I., *React. Kinet. Catal Lett.* **25,** 17 (1984).
38. Louwers, S. P. A., and Prins, R., *J. Catal.* **133,** 94 (1992).
39. Grunert, W., Stakheev, A. Y., Morke, W., Feldhaus, R., Anders, K., Shpiro, E. S., and Minachev, K. M., *J. Catal.* **135,** 269 (1992).
40. Okamoto, Y., Maezawa, A., and Imanaka, T., *J. Catal.* **120,** 29 (1989).
41. Hayden, T. F., and Dumesic, J. A., *J. Catal.* **103,** 366 (1987).
42. Topsøe, H., and Clausen, B. S., *Appl. Catal.* **25,** 273 (1986).
43. Burch, R., and Collins, A., *Appl. Catal.* **18,** 373 (1985).
44. Topsøe, N.-Y., Topsøe, H., and Massoth, F. E., *J. Catal.* **119,** 252 (1989).
45. Topsøe, H., Clausen, B. S., Topsøe, N.-Y., Pedersen, E., Niemann, W., Muller, A., Bogge, H., and Lengeler, B., *J. Chem. Soc., Faraday Trans. 1* **83,** 2157 (1987).
46. Shabtai, J., Nag, N. K., and Massoth, F. E., *in* "Proceedings, 9th International Congress on Catalysis, Calgary, 1988" (M. J. Phillips and M. Ternan, Eds.), Vol. 1, p. 1. Chem. Institute of Canada, Ottawa, 1988.
47. Ozkan, U. S., Zhang, L., Ni, S., and Moctezuma, E., *Energy Fuels,* in press.